Biaxial loading of offshore monopiles: numerical modelling

Brian B. Sheil[1*] and Bryan A. McCabe[2]

[1]Postdoctoral researcher, University of Oxford, Parks Road, Oxford OX1 3PJ, U.K. (formerly PhD Candidate, College of Engineering and Informatics, National University of Ireland, Galway, Ireland).

[2]Lecturer, College of Engineering and Informatics, National University of Ireland, Galway, Ireland.

**Corresponding author. Email: briansheil81@gmail.com; Tel.: +44 7894596969*

Abstract

In this paper, the FE software package PLAXIS 3D (2013) is used to examine the influence of biaxial lateral loading of a monopile foundation. Two different soil models are adopted to investigate the influence of state-dependent and anisotropic behaviour of soil on monopile response. A series of analyses were carried out where both cyclic and static lateral loads were applied to the pile. Results show that the consideration of biaxial loading significantly influences the pile head load-displacement response in addition to the development of significant accumulated displacements and co-existent soil loosening and densification. Moreover, predictions determined using a state-independent soil model are shown to be significantly non-conservative; these findings have important implications for environmental loading of offshore monopiles.

Keywords: Monopile, offshore, biaxial, lateral, numerical

Introduction

In the last decade, considerable effort has been made to produce more renewable energy, particularly offshore wind energy. The monopile remains the most common foundation system for offshore wind turbines and is suitable for water depths of over 30 metres. Traditional design methodologies for lateral loading on monopiles involve the use of p-y curves e.g. Maheshwari *et al.* (2005) and Zhang *et al.* (2014). However, this approach considers pile-soil interaction through a series of discrete springs for which the stiffnesses and ultimate resistances must be derived empirically (Su and Li 2013). Furthermore, the applicability of the p-y method to the analysis of larger diameter (i.e. greater than 3 m) piles remains unverified (Achmus *et al.* 2005).

Modern computational capability means that 3-D finite element (FE) analysis is becoming a feasible option for the design of monopiles under environmental loading, thus alleviating the expense associated with full-scale testing. This loading is multidirectional in nature, as cyclic loadings induced by wind and waves offshore are not necessarily coincident (Byrne and Houlsby 2003). However, the number of studies considering multidirectional loading of monopile foundations documented in the literature is limited.

Mayoral *et al.* (2005) reported the results of model piles in clay subject to a number of multi-directional displacement paths. The authors noted that the shape of the p-y curves was strongly dependent on both the pile head trajectory and the gap developed at the pile-soil interface. Levy *et al.* (2007) adopted a Winkler-type approach to investigate the influence of recent loading history on the lateral response of a single pile using local yield surfaces along the length of the pile. These authors noted that changes in lateral loading direction can have a significant influence on the pile load-displacement response.

Su (2012) conducted a number of laboratory tests on a single pile in sand to determine the response under both unidirectional (i.e. loading in one plane only) and multidirectional lateral loading. It was noted that, in general, the lateral resistance of the pile for the multidirectional cases was lower than a corresponding unidirectional case. This finding was later reiterated by Su and Li (2013) in light of a series of finite element analyses using a simplified state-dependent dilatancy model. All of these studies were limited to monotonic loading, however, and to the authors' knowledge there are no studies that have considered out-of-plane loads on the behaviour of monopiles subjected to cyclic lateral loads.

In this paper, the FE software package PLAXIS 3D 2013 (Plaxis bv. 2013) is used to examine the influence of multi-directional loading (static and cyclic) on the lateral response of a monopile foundation as used in offshore applications. The Hypoplastic soil model with inter-granular strain concept (Niemunis and Herle 1997; von Wolffersdorff 1996) capable of

accounting for small-strain stiffness nonlinearity, soil anisotropy and state-dependent behaviour was adopted for this study. In order to isolate the influences of soil anisotropy and soil state-dependency, a limited number of analyses were also undertaken using the elasto-plastic Hardening Soil model with small-strain stiffness (HSsmall). Both constitutive models were calibrated and validated using measured data from centrifuge tests on a monopile in Fontainebleau sand described by Giannakos *et al.* (2012). The results underline the importance of soil state-dependency when considering monopoles subjected to cyclic loading.

Finite Element modelling of monopiles

Reference case & modelling details

The geometric parameters presented in Fig. 1 serve as reference pile parameters for all FE analyses (Hypoplastic and HSsmall) in this paper; these are: length, L, of 14.6 m, diameter, D, of 0.72 m with wall thickness, t, of 60 mm and a Young's Modulus equal to 74 GPa. These parameters are deliberately consistent with prototype dimensions and properties modelled in centrifuge pile load tests described by Giannakos *et al.* (2012), carried out at 40*g*, which are modelled later in this paper. To simplify the modelling in this study, a solid cylindrical pile was used instead of a pipe pile with a Young's Modulus of 38 GPa, chosen to give an equivalent flexural rigidity, EI, of 505 MN m^2 to that of the pipe pile (where I is the section moment of area of the section) given a wall thickness, t, of 60 mm.

The lateral and bottom boundaries of the FE model were located sufficiently far from the monopile to avoid any influence on the FE output (see Fig. 1). Each analysis consisted of ~15,000 no. 10-noded tetrahedral elements; this was deemed to provide sufficient accuracy while also optimizing the computational efficiency in this study. In all analyses, the mesh was

refined in zones of high stresses and plastic deformations near the piles (details of the mesh refinement are shown in Fig. 2).

In PLAXIS, pile-soil damping is accommodated through soil hysteretic behaviour in cyclic loading. However, the magnitude of damping is dependent on the amplitude of the strain cycles and at very low strain amplitudes may be insignificant. A number of researchers have shown that at shear strain amplitudes of less than 0.01%, the damping is relatively constant with a value of approximately 3% (Kokusho et al. 1982; Okur and Ansal 2007; Vucetic and Dobry 1991). In light of this, additional Rayleigh damping is introduced to replicate the damping characteristics of real soils (Plaxis bv. 2013). Considering a 3% damping on the overall system, Rayleigh damping parameters were chosen as R_α=0.343 and R_β=8.68×10^{-2} for target frequencies of 1 Hz and 10 Hz (Giannakos 2013), where R_α and R_β determine the influence of mass and stiffness, respectively, in the damping of the system.

Analysis stages

The following are the analysis stages employed in this study:

(i) Initial stress generation by the K_0 procedure, a special calculation method available in PLAXIS.

(ii) 'Wished-in-place' pile installation reflected by changing appropriate elements to a linear elastic material with a Young's modulus of 38 GPa and a Poisson's ratio, ν, of 0.15. Sarkar and Maheshwari (2012) noted the importance of separation between pile and soil on pile-soil interaction; interface elements are therefore included in the model. In this study the change in stress owing to pile installation is not considered. However, the area of soil influenced by lateral pile loading is significantly greater

than the zone of soil that experiences pile installation effects (Achmus et al. 2009); therefore, this was not considered an unreasonable simplification.

(iii) Pile loading by placing lateral cyclic and/or static loads on the surface of the pile at the location shown in Fig. 1. Further details regarding the loading scenarios considered are discussed later in this paper.

(iv) Recording the pile displacement versus pile load relative to the start of loading.

Constitutive models

The hypoplastic model with inter-granular strain concept

For the purpose of this study, the Hypoplastic model with inter-granular strain concept was implemented as a user-defined soil model in PLAXIS (Gudehus et al. 2008). Hypoplasticity differs from classical elasto-plasticity in that no distinction between elastic and plastic deformations or yield and plastic potential surfaces is required. Van Wolffersdorff (1996) documented arguably the most popular hypoplastic model for the simulation of the behaviour of granular material. The hypoplastic model consists of two state variables, namely the current Cauchy stress **T** and the void ratio *e*. The hypoplastic constitutive equation is of the rate type and can be defined as follows:

$$\dot{\mathbf{T}} = \mathbf{F}(\mathbf{T}, e, \mathbf{D}) \tag{1}$$

where $\dot{\mathbf{T}}$ is the stress rate tensor, **F** is a tensor-valued function dependent on two variables: the stress **T** and the void ratio *e*, and **D** is the stretching rate.

Three distinct pressure-dependent void ratios are used; the parameter e_i determines the upper bound of the void ratio at its loosest possible state and decreases with increasing mean skeleton pressure p_s; e_d represents the lower bound to the void ratio and can be reached by cyclic shearing at small amplitude, also decreasing with mean skeleton pressure; e_c

corresponds to the critical void ratio. The granular hardness parameter, h_s, controls the change of limiting void ratios with the mean skeleton pressure:

$$\frac{e_i}{e_{i0}} = \frac{e_c}{e_{c0}} = \frac{e_d}{e_{d0}} = \exp\left[-\left(\frac{3p_s}{h_s}\right)^n\right] \quad (2)$$

where n is a material constant and controls the curvature of the oedometric compression curve. The failure surface of this model is equivalent to that of Matsuoka and Nakai (1974). Additional information on the formulation of this constitutive model is available elsewhere (Herle and Gudehus 1999; Niemunis and Herle 1997; von Wolffersdorff 1996).

The Hardening Soil model with small-strain stiffness

The Hardening Soil model with small-strain stiffness (HSsmall) is an elasto-plastic constitutive model capable of capturing small-strain stiffness nonlinearity; this model has been adopted herein to identify the influence of soil state-dependency and anisotropy which is captured by the Hypoplastic model. The HSsmall model implemented in PLAXIS is largely based on the original Hardening Soil (HS) model. The HS model has the advantage (over an elastic perfectly-plastic model) that the yield surface is not fixed in principal state but instead can expand due to plastic straining (Plaxis bv. 2013). It is an improvement on the Duncan-Chang hyperbolic model in that the theory of plasticity is used as opposed to the theory of elasticity. It also incorporates soil dilatancy and a yield cap although creep behaviour is not considered. Further details of the HS model are available elsewhere, e.g. Schanz *et al.* (1999), Sheil and McCabe (2014).

In contrast to the HS model, the HSsmall model accounts for small-strain stiffness nonlinearity and therefore this model is capable of capturing hysteresis in cyclic loading. The HSsmall model employs a form of the well-known Hardin and Drnevich (1972) relationship to describe the stress-strain behaviour of soils at small strains defined as:

$$\frac{G_s}{G_0} = \frac{1}{1+a\left|\frac{\gamma}{\gamma_{0.7}}\right|} \quad (3)$$

where G_0 is the initial (small-strain) shear modulus, G_s is the secant shear modulus, γ is the shear strain and $\gamma_{0.7}$ is the shear strain at which G_s has reduced to approximately $0.7G_0$, corresponding to a value of a=0.385 (Santos and Correia 2001). The degradation in small-strain stiffness is cut-off at the unloading-reloading shear modulus, G_{ur}, (see Fig. 3) which is defined by the unloading-reloading Young's modulus, E_{ur}, and Poisson's ratio, ν_{ur}, material parameters (Plaxis bv. 2013).

Parameter selection

Overview

The aim of this paper is to investigate the influence of multidirectional loads on the response of a monopile foundation. The Hypoplastic model with inter-granular strain concept is capable of capturing small-strain stiffness nonlinearity, anisotropy and state-independent behaviour of soil and represents the default constitutive model employed in this study. The ability of a more rudimentary soil model to simulate the likely behaviour of a monopile foundation subjected to offshore environmental loads is also of interest; the HSsmall model has been adopted for this purpose which is capable of simulating realistic small-strain stiffness nonlinearity. Both constitutive models have been calibrated and validated using centrifuge pile experiments in Fontainebleau sand documented elsewhere in the literature.

Centrifuge tests

Three different centrifuge pile experiments described by Giannakos *et al.* (2012) are modelled for the subsequent calibration and validation of the two soils models. The tests

differ by their cyclic loading characteristics; the parameters ζ_b and ζ_c are used in this study to characterize the harmonic loading and are defined as follows (LeBlanc et al. 2010):

$$\zeta_b = \frac{P_{max}}{P_{ult}} \quad (4a)$$

$$\zeta_c = \frac{P_{min}}{P_{max}} \quad (4b)$$

where P_{min} and P_{max} are the minimum and maximum horizontal loads, respectively, and P_{ult} is the load at pile failure. In this study, P_{ult} is defined as the load required to generate a pile head displacement of 0.1*D*. Tests P32, P344 and P330 represent values of ξ_c of 0.5, 0 and -1, respectively and are illustrated in Fig. 4. These sequences were used as the input loading in the centrifuge tests and therefore have also been adopted in the present FE simulations of these tests. Measured data from test P32 were used for the purpose of model calibration. Measured data from tests P344 and P330 were then used to validate the adopted pile/soil parameters. Further details regarding the tests are provided in Rosquoët *et al.* (2004), Gerolymos *et al.* (2009) and Giannakos *et al.* (2012).

Hypoplastic parameter calibration

The Hypoplastic parameters adopted for Fontainebleau sand in the present study are listed in Table 1. A value of 32° was chosen for the critical state friction angle, φ'_{cs} (Giannakos 2013). A value of 0.54 and 0.865 was adopted for parameters e_{d0} and e_{c0}, respectively by assuming $e_{d0} \approx e_{min}$ and $e_{c0} \approx e_{max}$ (Suchomel and Mašín 2009) where e_{min} and e_{max} are the minimum and maximum void ratios, respectively, determined from standard soil tests (Suchomel and Mašín 2009). The parameter e_{i0} was determined from the relationship $e_{i0} \approx 1.2 * e_{c0}$ (Suchomel and Mašín 2009).

The parameter n depends distinctly on the mean grain size, d_{50}, and non-uniformity, C_u, and can be approximated from the following relationship (Herle and Gudehus 1999):

$$n \approx 0.366 - 0.0341\left(\frac{C_u}{{d_{50}}^{0.33}}\right) \quad (5)$$

using values of 1.72 and 0.23 mm for C_u and d_{50}, respectively (Pra-Ai 2013), yielding a value of 0.28 for n. The parameter β influences the soil shear stiffness; in the absence of specific triaxial tests, a default value of 1.0 was adopted which is suitable for most sands (Suchomel and Mašín 2009). The parameter α controls the peak friction angle; a value of 0.3 was selected to correspond to a peak friction angle of 42° (Giannakos et al. 2012). The parameter h_s can be obtained by curve-fitting to the measured oedometric compression curve of a loose sample; since this information was not available, this parameter was instead calibrated to fit the measured virgin load-displacement response (see Fig. 5).

The remaining parameters relate to the intergranular strain concept. The default values for m_T, R and χ documented by Niemunis and Herle (1997) were also retained in this study. The parameters m_R and β_r determine the stiffness upon strain reversal and the stiffness degradation characteristics, respectively; these values were determined through curve-fitting to the measured load-displacement response during cyclic loading as shown in Fig. 5.

In addition to material parameters, the interface parameters must also be 'user-defined'. The interface was modelled as a Mohr-Coulomb material with parameters defined using an interface strength reduction factor, R_{inter}, in conjunction with the default relationships adopted in PLAXIS:

$$tan\delta = R_{inter} tan\varphi_{soil} \quad (6a)$$

$$E_{oed,i} = R_{inter}^2 E_{oed,soil} \quad (6b)$$

where δ is the interface friction angle, φ'_{soil} is the friction angle of the adjacent soil and $E_{oed,i}$ and $E_{oed,soil}$ are the oedometric moduli of the interface and adjacent soil, respectively (Plaxis

bv. 2013). A value of 0.9 was chosen for R_{inter} at the steel-soil interface (Tiwari et al. 2010). This involved simulating an oedometer test using PLAXIS soil test facility using the Hypoplastic model to determine the value of $E_{oed,soil}$ at a particular reference pressure, p_{ref}.

HSsmall parameter calibration

The HSsmall parameters adopted for the simulation of Fontainebleau sand are listed in Table 2. In PLAXIS, the critical state friction angle, φ'_{cv}, is automatically computed from input data on the peak friction angle, φ'_p, and dilatancy angle, ψ. Therefore a value of φ'_p =41.8° was chosen to correspond to the peak friction angle (Giannakos et al. 2012). A value of ψ =11° was calculated from the empirical relationship developed by Bolton (1986) defined as follows:

$$\varphi'_p = \varphi'_{cv} + 0.8\psi \quad (7)$$

A value of 1 kPa was chosen for the soil cohesion, c', for the sake of numerical stability. A value of 80 MPa was chosen for G_0 corresponding to a reference pressure, p', of 100 kPa (~1 atm); these were based on measured values reported by Giannakos *et al.* (2012). A default value of 0.2 was chosen for the unloading/reloading Poisson's ratio, v_{ur}. Reference was made to the measured shear modulus degradation curves for Fontainebleau sand reported by Georgiannou et al. (2008) for the selection of $\gamma_{0.7}$ =4×10^{-3}. A value of 0.9 was again chosen for R_{inter} at the steel-sand interface.

The secant shear modulus in triaxial compression, E_{50}^{ref}, was derived by calibrating PLAXIS predictions to the measured load-displacement response of test P32 during primary loading. Similarly, the unloading/reloading stiffness, E_{ur}^{ref}, was derived from calibration to the measured unload-reload response of test P32. Values of 18 MPa and 45 MPa were chosen for E_{50}^{ref} and E_{ur}^{ref}, respectively; the fit between the predicted and measured load-displacement

responses is illustrated in Fig. 6. It can be seen that the HSsmall captures the primary loading response very well. In addition, the HSsmall also replicates the hysteresis loops during unload-reload cycles relatively well.

Validation of constitutive models

For the purpose of validating the parameters adopted herein, FE predictions of the load displacement response have been compared to measured data from both test P344 (Fig. 7) and test P330 (Fig. 8). From Figs. 7a and 7b, PLAXIS appears to predict the initial load-displacement stiffness very well for the HSsmall and Hypoplastic model, respectively; the total accumulated displacements at the end of the test are slightly under-predicted by the HSsmall model which should be expected from a state-independent model. For test P330 in Fig. 8, slight over-predictions of the initial load-displacement stiffness are obtained using both model; the hysteresis loops in cyclic loading are relatively well captured, however. These results confirm that predictions of monopile behaviour subjected to small cycle numbers are satisfactory.

Loading scenarios

As mentioned, the majority of studies investigating cyclic lateral loading of a monopile relate to loading in one plane (i.e. unidirectional loading), although Byrne and Houlsby (2003) noted that environmental loadings of monopiles offshore are typically multidirectional in nature. These effects were examined by considering two different sets of analyses: (i) unidirectional analyses where only a harmonic load was applied to the pile (denoted the *x*-direction; see Fig. 9a) and (ii) multidirectional analyses where both harmonic (*x*-direction) and static loads (*z*-direction) were applied to the pile with incident angles of 90° (see Fig. 9b).

285 The various loading paths imposed for the multidirectional analyses are illustrated in Fig. 10
286 where P_x and P_z are the applied horizontal loads in the *x*-direction and *z*-direction,
287 respectively. The initial load-displacement response prior to cyclic loading is denoted the
288 'virgin loading path' which makes an angle ϑ with the *x*-direction (direction of cyclic
289 loading). For example, an angle of $\vartheta = 0°$ denotes loading in the *x*-direction only. It can be
290 seen that the initial loading angle, ϑ, varies from 53° to 90°; in light of this, the influence of ϑ
291 on the initial load-displacement is also examined in the subsequent sections. The subsequent
292 cyclic loading path is shown in dashed lines.

293 A harmonic frequency of 0.1 Hz is of particular interest in the design of offshore monopiles
294 which corresponds to the Pierson and Moskowitz (1964) dynamic wave load spectrum for
295 North UK Sea locations (Bhattacharya et al. 2012); this frequency has therefore been adopted
296 in this study. LeBlanc *et al.* (2010) reported the range $0.3 \leq \zeta_b \leq 0.5$ as being of most interest
297 to geotechnical engineers where the lower bound corresponds to fatigue limit state and the
298 upper bound corresponds to serviceability limit state. The authors adopt serviceability limit
299 state (i.e. $\zeta_b = 0.5$) as the basis for the harmonic loading in the present study which
300 corresponds to 100 load cycles, *n*, during the lifetime of the wind turbine (Byrne and Houlsby
301 2003). There is little guidance on typical values of ζ_c for an offshore monopile; so the range -
302 $1 \leq \zeta_c \leq 0.5$ has been considered herein in the interest of completeness.

303 For the sake of simplicity, both the harmonic and static loads were applied to the pile at the
304 same elevation; the value of *e* was chosen as 0.13*L* (see Fig. 1) and maintained throughout
305 the study, where *L* is the embedment length of the pile. The magnitude of the static load,
306 P_{static}, was arbitrarily chosen to equal the maximum load induced by the harmonic loads, i.e.
307 $P_{static} = P_{max}$.

308 The initial void ratio, e_0, was derived using the following relationship:

309 $$I_{D0} = \frac{e_{max} - e_0}{e_{max} - e_{min}} \approx \frac{e_i - e_0}{e_i - e_c} \quad (8)$$

310 where I_{D0} is the initial relative density. The range of values of I_D encountered for seabed
311 floors is quite broad. After initial deposition of suspended sediments, the soil is loose with I_D
312 most commonly of the order of ~35%; however, after a number of storms and subsequent
313 settlement and densification of the seabed, values of I_D of up to 100% may arise (Teh et al.
314 2006). In light of this, a default value of I_{D0} = 0.35 was used for this study with a limited
315 number of analyses with I_{D0} = 0.7 included for comparison.

316

317 **Parametric study – PLAXIS results**

318 *Load-displacement (P-δ) response*

319 In Figs. 11-13, the normalised load-displacement (P-δ) responses at the pile head, in the *x*-
320 direction have been plotted (see Fig. 9), for both a unidirectional analysis (no static load) and
321 multidirectional analysis (with static load) and using the HSsmall and Hypoplastic soil
322 models. Values of ζ_c of 0.5, 0 and -1 (defined in Figs. 5a, 5b and 5c, respectively) have been
323 adopted in Figs. 11, 12 and 13, respectively.

324 For a value of ζ_c=0.5 in Fig. 11, predictions of the multidirectional response (ϑ=53°)
325 determined using both models appear to exhibit notably lower P-δ stiffnesses in virgin
326 loading compared to their respective unidirectional analyses. This is consistent with the
327 findings of Su (2012; 2013) who reported lower P-δ stiffnesses for multi-directional pile head
328 trajectories compared to traditional unidirectional analyses in virgin loading. Interestingly,
329 both models predict slightly different behaviour during the course of the cyclic loading. After
330 *n*=100 cycles, the HSsmall model predicts larger displacements for the multidirectional case;
331 in contrast, the Hypoplastic model predicts slightly larger displacements for the unidirectional
332 case. These findings are largely replicated in Fig. 12; the Hypoplastic model predicts

significantly larger displacements for the multidirectional case compared to the state-independent HSsmall predictions. In addition, it can be seen that an increase in ϑ to 63° causes a further reduction in the initial multidirectional load-displacement response predicted by the Hypoplastic model.

In contrast to these findings, for a value of ζ_c=-1 in Fig. 13, the HSsmall model predicts a similar response for both the uni-directional and multi-directional loading cases. Hypoplastic predictions indicate a significantly greater accumulation of displacements for the multidirectional case, however. In light of the results presented heretofore, it is clear that the 'out-of-plane' static load has a significant influence on the P-δ response; however, these differences are dependent not only the cyclic loading characteristics but also on a constitutive model capable of accurately simulating complex loading regimes.

Pile head trajectories

As mentioned, there is little guidance in the literature on typical pile head trajectories for multidirectional loading of offshore monopiles. Fig. 14 illustrates pile head trajectories for multidirectional loading where the value of ζ_c has again been varied from 0.5 to -1; predictions determined using both the HSsmall and Hypoplastic model are presented in Fig. 14a and Fig. 14b, respectively. It should be noted that the HSsmall model does not predict accumulation of displacements due to its omission of soil state dependency; therefore this model is only capable of predicting alternating plasticity while the Hypoplastic model is also capable of considering ratcheting. The results presented in Fig. 14 show a progressive accumulation of displacements in the *x*-direction due to cyclic loading for ζ_c=0 and ζ_c=0.5; as expected, the accumulation of displacements for ζ_c=0 predicted by the HSsmall model are

356 noticeably lower than the corresponding Hypoplastic results, highlighting the influence of
357 ratcheting.

358 A value of ζ_c=-1 results in only a slight increase in displacements in the *x*-direction using
359 both models. Predictions for ζ_c=-1 in Fig. 14a at values of δ_z/D>~8.5% appear unreliable and
360 could be due to mesh deterioration at large deformations since geometric nonlinearity is not
361 considered. The magnitude of the accumulated displacement in the *z*-direction is particularly
362 interesting where a value of ζ_c=-1 exhibits the greatest 'out-of-plane' displacement due to the
363 static loading (predictions determined using the Hypoplastic model reach failure in the *z*-
364 direction).

365 The value of I_{D0} has a notable influence on predictions of the pile head trajectories
366 determined using the Hypoplastic model (see Fig. 15). While the overall pile head trajectories
367 are similar for both values of I_{D0}, only the loose sand analysis reaches failure (i.e. 10%*D*).
368 These results, in particular, illustrate the limitation associated with unidirectional analyses
369 where the accumulated displacements in the *z*-direction would be neglected.

370

371 *Accumulated displacements*

372 In Fig. 16, the variation in the accumulated 'absolute' displacements have been plotted in the
373 form of $|\delta|_N/|\delta|_1$ against *N* where $|\delta|_N$ and $|\delta|_1$ are the absolute displacement after *N* cycles
374 and 1 cycle, respectively and $|\delta| = \sqrt{\delta_x^2 + \delta_z^2}$. From an examination of the results presented
375 in Fig. 16 determined using the Hypoplastic model, the following conclusions may be drawn:

376 • Predictions for ζ_c=-1 with multidirectional loading form a clear upper bound for the
377 accumulation of displacements.
378 • Multidirectional loading increases the accumulation of displacements for all cases
379 except for ζ_c=0.5 where predictions are very similar to the unidirectional case.

- Some of the trends become 'wavier' for $N \geq 20$; due to the very small accumulation of displacements at higher values of N, the possibility that numerical errors begin to have an influence on these trends remains open to question.

The influence of ζ_c on the accumulation of 'out-of-plane' displacements (i.e. $|\delta_z|_N/|\delta_z|_1$) during multidirectional loading is considered further in Fig. 17. It is clear from this figure that a value of ζ_c induces significantly larger out-of-plane displacements thus explaining the differences observed in the previous figure. Numerous experimental studies reported in the literature have documented significant influences of the shape of the strain paths on the accumulation of displacements; Ishihara and Yamazaki (1980) noted that the stress amplitude during cyclic loading plays a particularly important role. The authors therefore attribute the increased accumulation of displacements associated with a value of ζ_c=-1 to the larger stress amplitudes applied to the pile.

In Fig. 18, the influence of the sand type on accumulated displacements is considered where predictions determined using the present Fontainebleau parameters have been compared to those obtained using parameters for Hochstetten sand documented by Niemunis and Herle (1997). While results are relatively similar for values of ζ_c of 0.5 and 0, the sand properties have a clear influence on the accumulation of displacements for ζ_c=-1.

Furthermore, the influence of the adopted constitutive model is examined in more detail in Fig. 19 for the multidirectional loading case. The Hypoplastic model predicts much higher accumulated displacements in all cases compared to the HSsmall model except for ζ_c=0.5. In light of this, the HSsmall model may only be considered to give reasonable predictions of accumulated displacements for one-way loading of a monopile in sand; it is obvious that predictions for alternative scenarios will lead to non-conservative predictions.

Soil densification

Progressive soil densification with increasing N has important ramifications for the performance of monopiles supporting offshore wind turbines. Significant densification can cause deviations in the natural frequency of the pile-soil system which may lead to resonance with the external excitation forces acting on the system. As mentioned, the HSsmall model is state-independent and therefore cannot capture ratcheting behaviour due to soil densification. Therefore, any accumulated displacements are a result of soil stiffness degradation surrounding the pile. Fig. 20 presents a three-dimensional illustration of the stiffness degradation predicted by the HSsmall model. Interestingly, the HSsmall-predicted stiffness degradation contours are conical in shape; this is consistent with the 'cone-shaped' shear strain contours for a model pile (in loose sand) based on PIV measurements documented by Hajialilue-Bonab *et al.* (2013). Moreover, it can be seen from Fig. 21 that multidirectional loading has a significant influence on the stiffness degradation contours surrounding the pile.

In the subsequent figures, the progressive densification of the soil surrounding the pile, predicted by the Hypoplastic model, is examined using contours of I_D which were derived from PLAXIS output of the current void ratio, e. In Fig. 22, the influence of both multidirectional loading and the value of N on I_D at ground level are examined. It can be seen that there is significant densification of the soil surrounding the pile even after N=10 with further densification obvious at N=100 for multidirectional loading. It is also clear that the nature of the loading has an influence on the soil densification surrounding the soil thus explaining the increased accumulated displacements observed in the previous section.

Conclusions

In this paper, a numerical study of multidirectional loading of a single pile in Fontainebleau sand has been presented using the Hypoplastic model in conjunction with PLAXIS 3D 2013. A limited number of analyses using the state-independent, isotropic Hardening Soil model with small-strain stiffness have also been included for comparison. The authors have arrived at the following conclusions:

(a) The 'out-of-plane' static load caused significant changes to the load-displacement response of the pile in the direction of cyclic loading; these effects were not only dependent on the cyclic loading characteristics but also heavily dependent on the adopted constitutive model.

(b) Similarly, the 'out-of-plane' loading also induced noticeable accumulated displacements to occur in the same direction (denoted the *z*-direction) which would not be captured by a corresponding unidirectional analysis. A value of ζ_c=-1 (representing two-way loading) produced the largest accumulation of displacements and is much more severe for looser soils; this was attributed to the larger stress amplitudes applied to the pile during this particular analysis.

(c) The load level corresponding to ζ_c=0.5 was documented by LeBlanc *et al.* (2010) as representing serviceability limit state and is exceeded approximately 100 times during the lifetime of a monopile foundation; this study shows that failure may occur due to an out-of-plane static load before 100 cycles.

(d) The HSsmall model only gave reasonable predictions of accumulated displacements for one-way loading; simulation of any other scenario will lead to non-conservative predictions.

(e) Significant densification surrounding the pile was shown to occur even after 10 cycles; multidirectional loading induced additional densification thus contributing to the increased accumulation of displacements.

The findings of the present study highlight the importance of careful consideration of both the environmental loading characteristics and subsequent constitutive modelling of offshore monopiles. In particular, the authors have highlighted that the consideration of environmental loading of a monopile in one plane only is not sufficient; out-of-plane loads can induce significant accumulation of displacements which may well lead to failure.

References

Achmus, M., Abdel-Rahman, K., and Peralta, P. "On the design of monopile foundations with respect to static and quasi-static cyclic loading." *Proc., Proceedings of the Offshore Wind Energy Conference*.

Achmus, M., Kho, Y.-S., and Abdel-Rahman, K. (2009). "Behavior of monopile foundations under cyclic lateral load." *Comput Geotech*, 36, 725–735.

Bhattacharya, S., Cox, J. A., Lombardi, D., and Muir Wood, D. (2012). "Dynamics of offshore wind turbines supported on two foundations." *Proceedings of the ICE - Geotechnical Engineering*, 166(GE2), 159-169.

Bolton, M. D. (1986). "The strength and dilatancy of sands." *Géotechnique*, 36(1), 65-78.

Byrne, B. W., and Houlsby, G. T. (2003). "Foundations for offshore wind turbines." *Philosophical Transactions of the Royal Society of London, Series A*, 361, 2909-2930.

Georgiannou, V. N., Tsomokos, A., and Stavrou, K. (2008). "Monotonic and cyclic behaviour of and under torsional loading." *Géotechnique*, 58(2), 113-124.

Gerolymos, N., Escoffier, S., Gazetas, G., and Garnier, J. (2009). "Numerical modeling of centrifuge cyclic lateral pile load experiments." *Earthquake Engineering and Engineering Vibration*, 8(1), 61-76.

Giannakos, S. (2013). "Contribution to the static and dynamic lateral response of piles."PhD Thesis, National Technical University of Athens.

Giannakos, S., Gerolymos, N., and Gazetas, G. (2012). "Cyclic lateral response of piles in dry sand: Finite element modeling and validation." *Comput Geotech*, 44, 116-131.

Gudehus, G., Amorosi, A., Gens, A., Herle, I., Kolymbas, D., Mašín, D., Muir Wood, D., Nova, R., Niemunis, A., Pastor, M., Tamagnini, C., and Viggiani, G. (2008). "The soilmodels.info project." *International Journal for Numerical and Analytical Methods in Geomechanics*, 32(12), 1571-1572.

Hajialilue-Bonab, M., Sojoudi, Y., and Puppala, A. J. (2013). "Study of strain wedge parameters for laterally loaded piles." *International Journal of Geomechanics*, 13(2), 143-152.

Hardin, B. O., and Drnevich, V. P. (1972). "Shear modulus and damping in soils: Design equations and curves." *Proc. ASCE: J Soil Mech Found Division*, 98(SM7), 667-692.

Herle, I., and Gudehus, G. (1999). "Determination of parameters of a hypoplastic constitutive model from properties of grain assemblies." *Mechanics of cohesive-frictional materials*, 4(5), 461-486.

Ishihara, K., and Yamazaki, F. (1980). "Cyclic simple shear tests on saturated sand in multi-directional loading." *Soils and Foundations*, 20(1), 45-59.

Kokusho, T., Yoshida, Y., and Esashi, Y. (1982). "Dynamic properties of soft clays for wide strain range." *Soils and Foundations*, 22(4), 1-18.

LeBlanc, C., Houlsby, G. T., and Byrne, B. W. (2010). "Response of stiff piles in sand to long-term cyclic lateral loading." *Géotechnique*, 60(2), 79-90.

Levy, N. H., Einav, I., and Randolph, M. F. (2007). "Effect of recent load history on laterally loaded piles in normally consolidated clay." *International Journal of Geomechanics*, 7(4), 277-286.

Maheshwari, B. K., Truman, K. Z., Gould, P. L., and El Naggar, M. H. (2005). "Three-dimensional nonlinear seismic analysis of single piles using finite element model: Effects of plasticity of soil." *International Journal of Geomechanics*, 5(1), 35-44.

Matsuoka, H., and Nakai, T. (1974). "Stress-deformation and strength characteristics of soil under three different principal stresses." *Proceedings of the Japanese Society of Civil Engineers*, 232, 59-70.

Mayoral, J. M., Pestana, J. M., and Seed, R. B. (2005). "Determination of multidirectional p-y curves for soft clays." *Geotechnical Testing Journal*, 28(3), 1-11.

Niemunis, A., and Herle, I. (1997). "Hypoplastic model for cohesionless soils with elastic strain range." *Mechanics of cohesive-frictional materials*, 2(4), 279-299.

Okur, D. V., and Ansal, A. (2007). "Stiffness degradation of natural fine grained soils during cyclic loading." *Soil Dynamics and Earthquake Engineering*, 27(9), 843-854.

Pierson, W. J., and Moskowitz, L. (1964). "A proposed spectral form for fully developed wind seas based on the similarity theory of SA Kitaigordskii." *Journal of Geophysical Research*, 69(24), 5181-5190.

Plaxis bv. (2013). *Plaxis 3D Version 2013, Reference Manual*, Delft, The Netherlands.

Pra-Ai, S. (2013). "Behaviour of soil-structure interfaces subjected to a large number of cycles. Application to piles."PhD Thesis, University of Grenoble.

Rosquoët, F., Garnier, J., Thorel, L., and Canepa, Y. "Horizontal cyclic loading of piles installed in sand: study of the pile head displacement and maximum bending moment." *Proc., Proceedings of the International Conference on Cyclic Behaviour of Soils and Liquefaction Phenomena*, Taylor & Francis, 363-368.

Santos, J. A., and Correia, A. G. "Reference threshold shear strain of soil. Its application to obtain a unique strain-dependent shear modulus curve for soil." *Proc., Proceedings of the 15th International Conference on Soil Mechanics and Geotechnical Engineering*, 267-270.

Sarkar, R., and Maheshwari, B. K. (2012). "Effects of separation on the behavior of soil-pile interaction in liquefiable soils." *International Journal of Geomechanics*, 12(1), 1-13.

Schanz, T., Vermeer, P. A., and Bonnier, P. G. "The hardening soil model: Formulation and verification." *Proc., Beyond 2000 in computational geotechnics. Ten Years of PLAXIS International. Proceedings of the international symposium, Amsterdam, March 1999.*, A.A.Balkema, 281-296.

Sheil, B. B., and McCabe, B. A. (2014). "A finite element based approach for predictions of rigid pile group stiffness efficiency in clays." *ACTA Geotechnica*, 9, 469-484.

Su, D. (2012). "Resistance of short, stiff piles to multidirectional lateral loadings." *Geotechnical Testing Journal*, 35(2).

Su, D., and Li, J. H. (2013). "Three-dimensional finite element study of a single pile response to multidirectional lateral loadings incorporating the simplified state-dependent dilatancy model." *Computers and Geotechnics*, 50, 129-142.
Suchomel, R., and Mašín, D. (2009). "Calibration of an advanced soil constitutive model for use in probabilistic numerical analysis." *Proc. Int. Symposium on Computational Geomechanics (ComGeo I)*Juan-les-Pins, France, 265-274.
Teh, T. C., Palmer, A. C., Bolton, M. D., and Damgaard, J. S. (2006). "Stability of submarine pipelines on liquefied seabeds." *Journal of Waterway, Port, Coastal, and Ocean Engineering*, 132(4), 244-251.
Tiwari, B., Ajmera, B., and Kaya, G. (2010). "Shear strength reduction at soil structure interface." *Advances in Analysis, Modelling and Design*, ASCE, Florida.
von Wolffersdorff, P.-A. (1996). "A hypoplastic relation for granular materials with a predefined limit state surface." *Mechanics of cohesive-frictional materials*, 1, 251-271.
Vucetic, M., and Dobry, R. (1991). "The effect of soil plasticity on cyclic response." *ASCE Journal of Geotechnical Engineering*, 117(1), 89-107.
Zhang, L., Zhao, M., and Zou, X. (2014). "Behavior of laterally loaded piles in multilayered soils." *International Journal of Geomechanics*, 15(2).

Table 1 Hypoplastic with inter-granular strain parameters for Fontainebleau sand

Sat weight density γ_{sat} (kN/m^3)	18.5
Unsaturated weight density γ_{unsat} (kN/m^3)	16.5
Critical state friction angle, φ' (°)	32
Granular hardness, h_s (GPa)	0.4
Material constant, n	0.28
Minimum void ratio after cyclic shearing at small amplitude, e_{d0} ($\approx e_{min}$)	0.54
Critical void ratio, e_{c0} ($\approx e_{max}$)	0.865
Maximum void ratio during isotropic compression, e_{i0}	1.04
Material constant, α	0.3
Material constant, β	1.0
Maximum value of intergranular strain, R	1×10^{-3}
Material constant, m_R	8
Material constant, m_T	2.0
Evolution of intergranular strain, β_r	0.3
Parameter controlling stiffness degradation during monotonic deformation, χ	6

561 **Table 2** HSsmall parameters for Fontainebleau sand

Sat weight density γ_{sat} (kN/m^3)	18.5
Unsaturated weight density γ_{unsat} (kN/m^3)	16.5
Friction angle, φ' (°)	33
Dilatancy angle, ψ (°)	8
Cohesion, c' (kPa)	1.0
Coefficient of lateral earth pressure, K	0.5
Initial (small-strain) shear modulus, G_0 (Mpa)	85
Shear strain corresponding to 0.7G_0, $\gamma_{0.7}$	4×10^{-3}
Tangent oedometric stiffness, $^{*}E'_{oed}{}^{ref}$ (Mpa)	18
Secant stiffness in drained triaxial test, $E'_{50}{}^{ref}$ (Mpa)	18
Unloading/reloading stiffness, $E'_{ur}{}^{ref}$ (Mpa)	45
Unloading/reloading Poisson's ratio, ν_{ur}	0.2
Reference pressure for stiffness, p_{ref} (kPa)	100
Power for stress-level dependency of stiffness, m	0.5
Interface strength reduction factor, R_{inter}	0.9

562 $^{*}E_{oed}{}^{ref}$ set equal to $E_{50}{}^{ref}$ in the absence of an appropriate reference

563

564

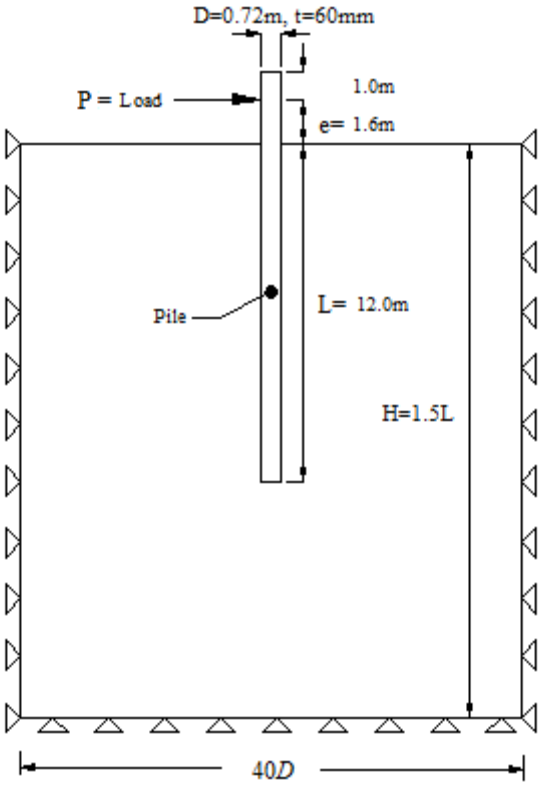

565

566 **Fig. 1** Details of finite element model

567

568

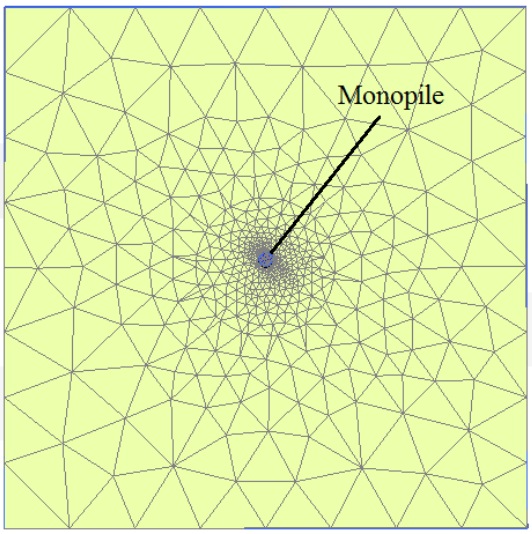

569

570

571 **Fig. 2** Plan view of mesh refinement

572

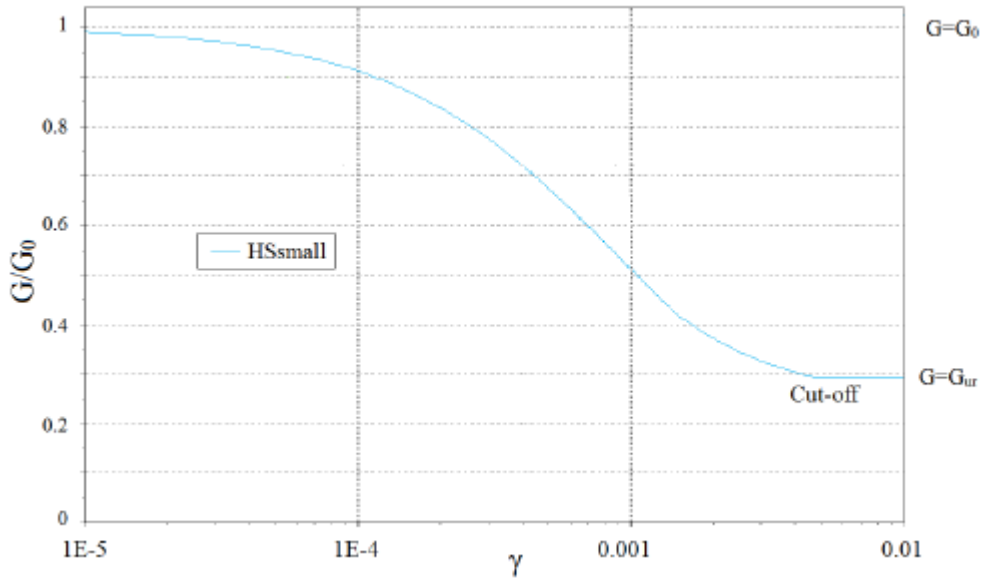

573
574 **Fig. 3** Illustration of small-strain stiffness lower bound for HSsmall model

575

576

577

578

579

580

581

582

583

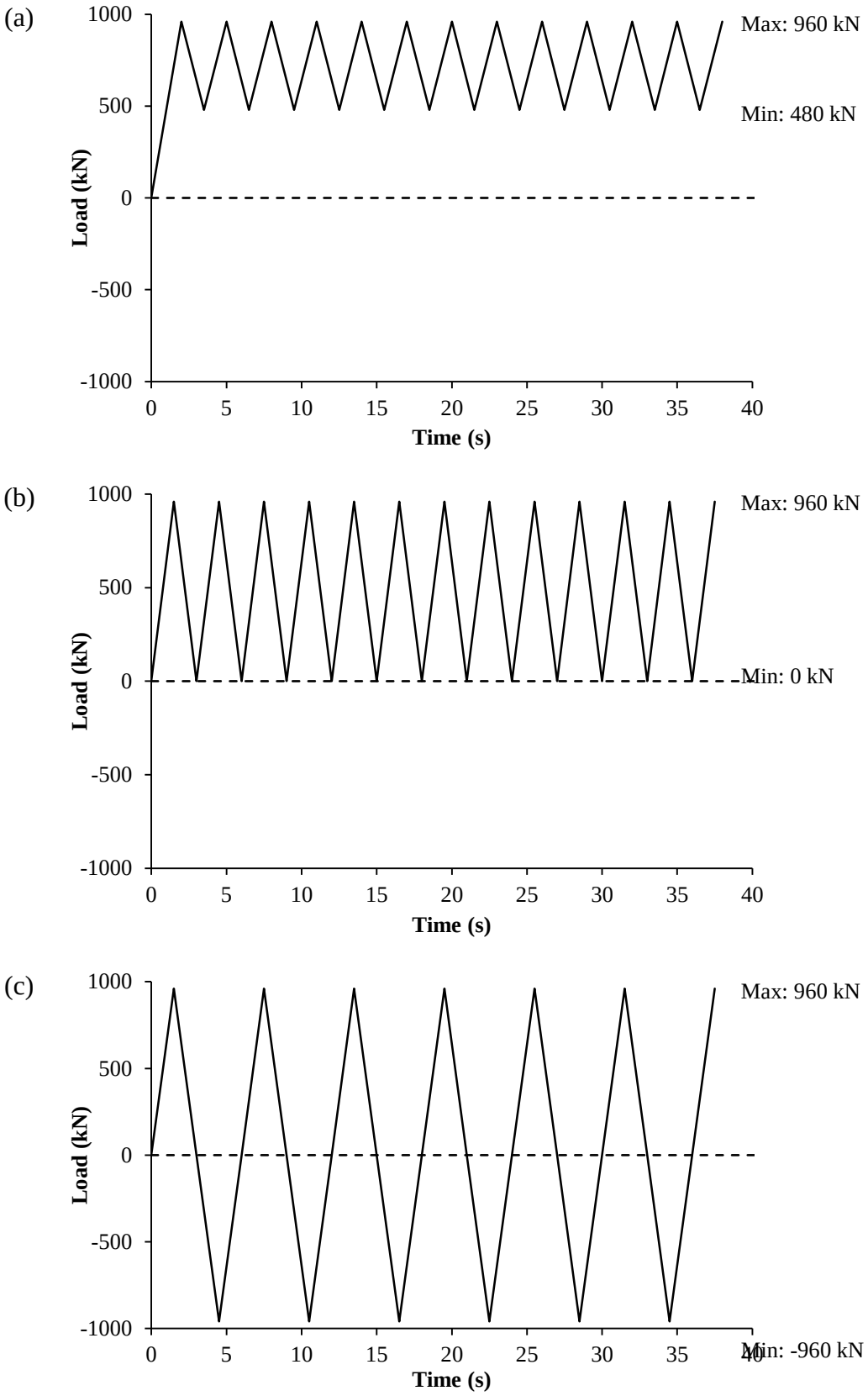

584

585 **Fig. 4** Loading sequence and FE dynamic input for tests (a) P32 (ζc=0.5) (b) P344 (ζc=0) and
586 (c) P330 (ζc=-1)

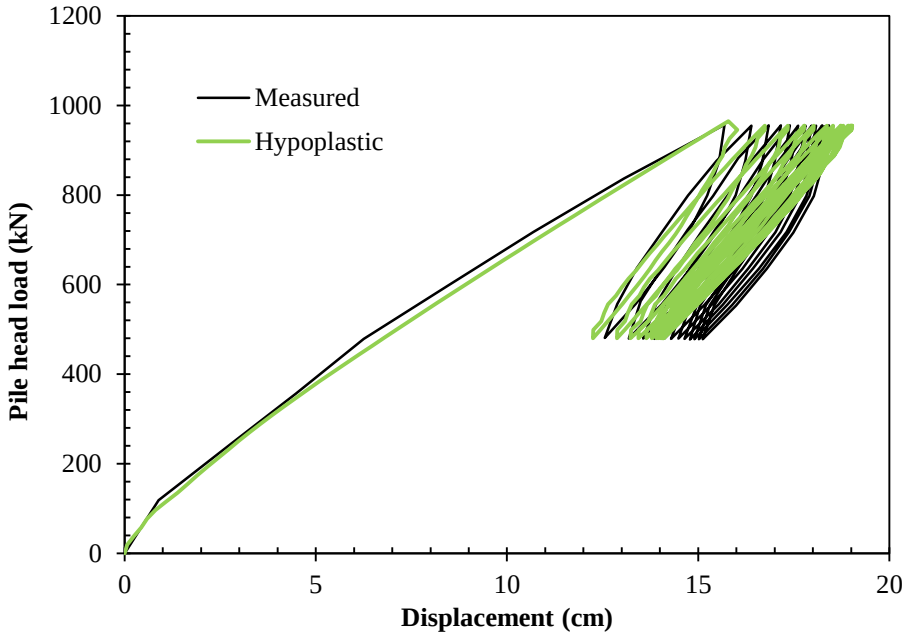

Fig. 5 Comparison between measured and predicted load-displacement responses for test P32; Hypoplastic

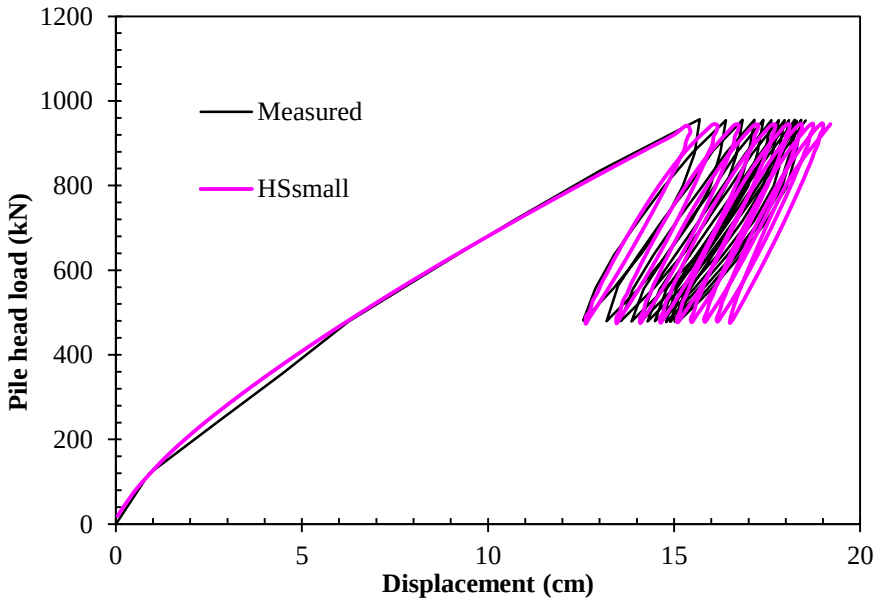

Fig. 6 Comparison between measured and predicted load-displacement responses for test P32; HSsmall

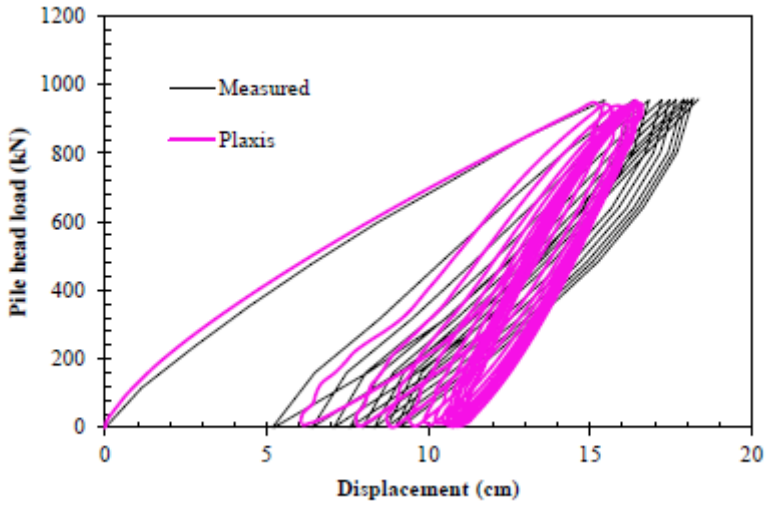

595

596

597 **Fig. 7** Comparison between measured and predicted load-displacement responses for test P344

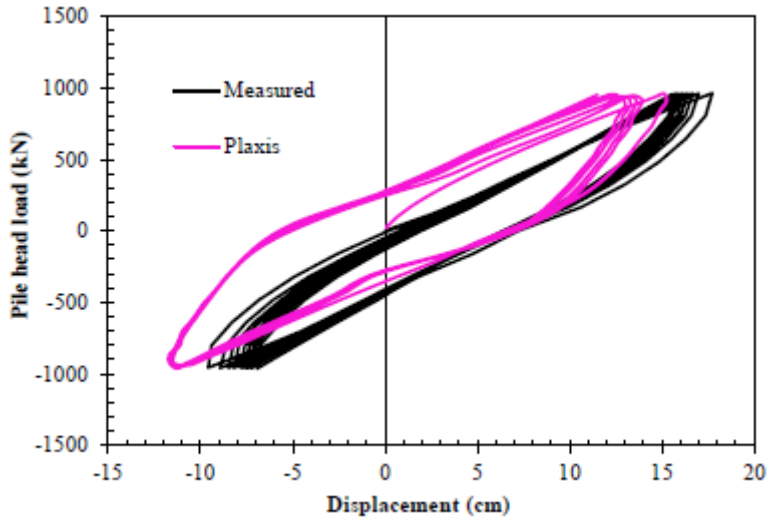

598

599

600 **Fig. 8** Comparison between measured and predicted load-displacement responses for test P330

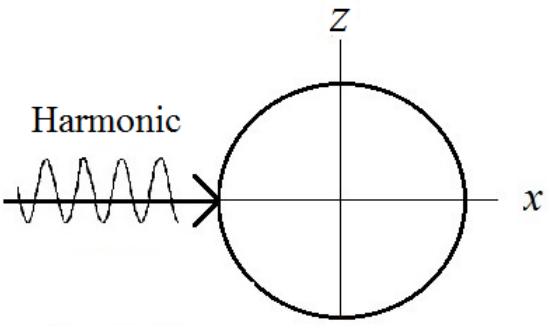

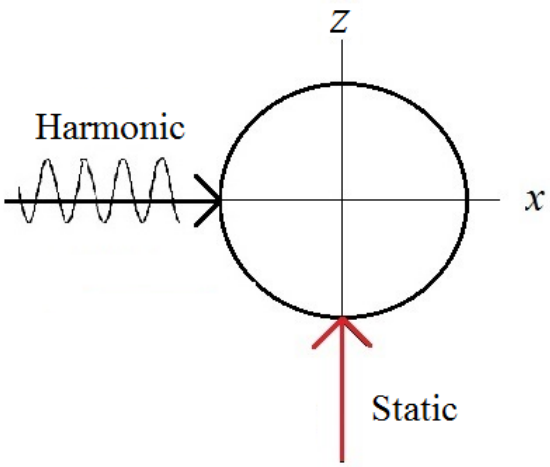

Fig. 9a Unidirectional analysis (no static load)

Fig. 9b Multidirectional analysis (with static load)

601
602

(a) (b) (c)

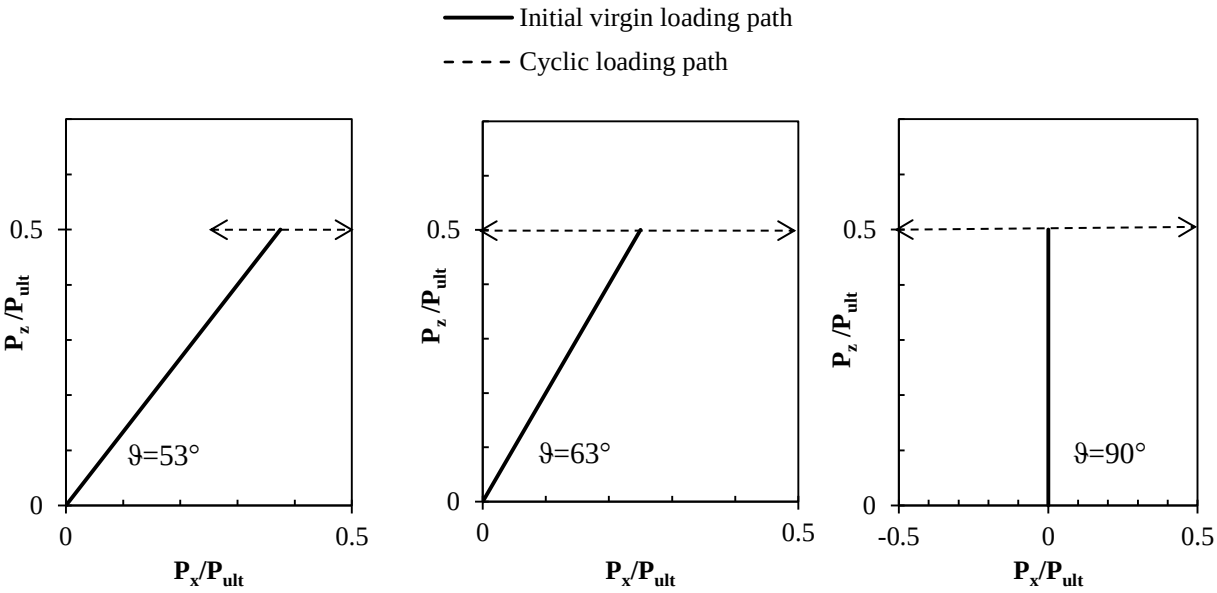

603

604 **Fig. 10** Multidirectional loading paths for (a) ζ_c =0.5, (b) ζ_c =0 and (c) ζ_c =-1

605

606

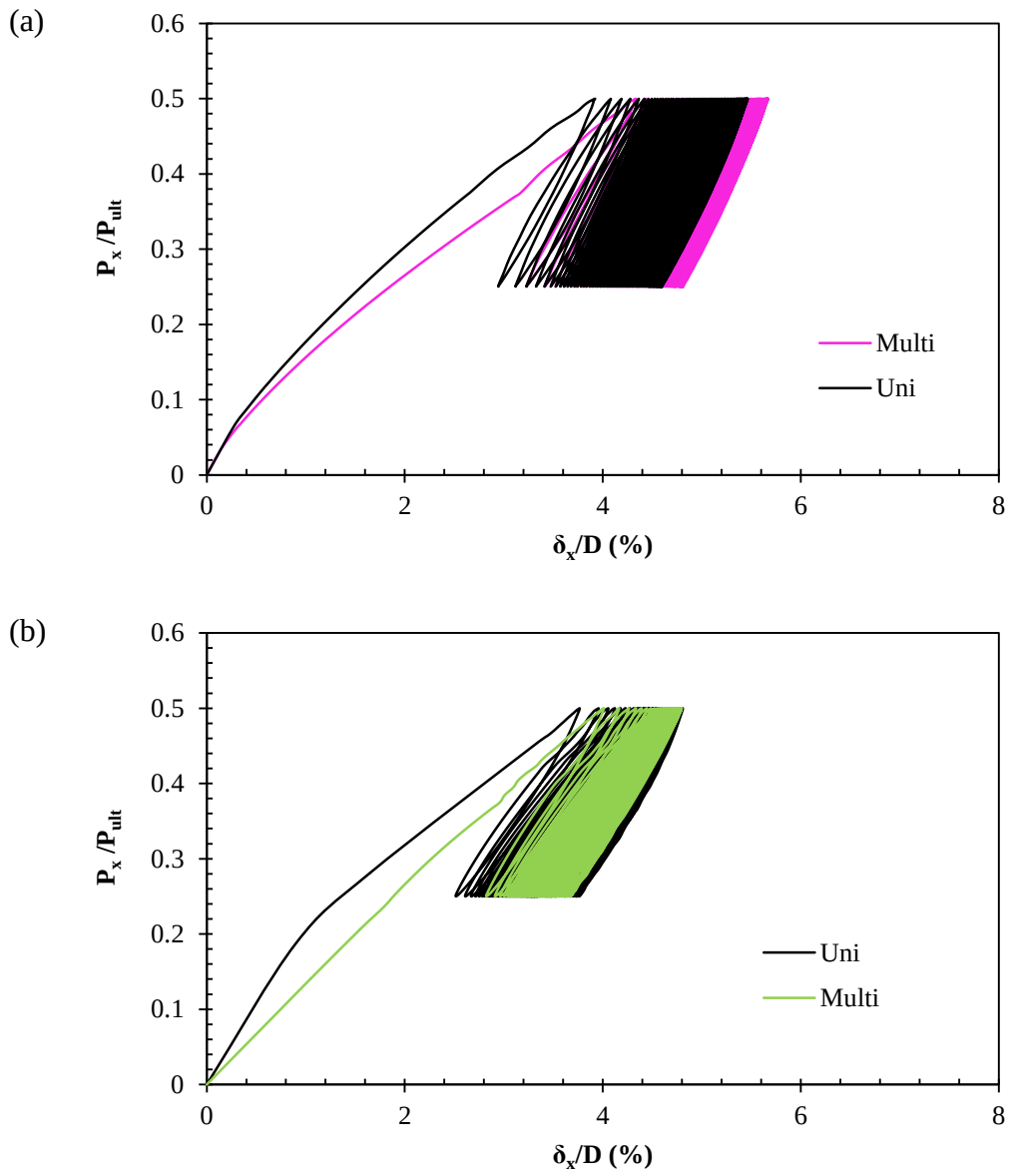

607 **Fig. 11** Comparison of unidirectional and multidirectional P-δ response in the *x*-direction for
608 ζ_c=0.5 using (a) the HSsmall model and (b) the Hypoplastic model, I_{D0}=0.35

609

610

611

612

613

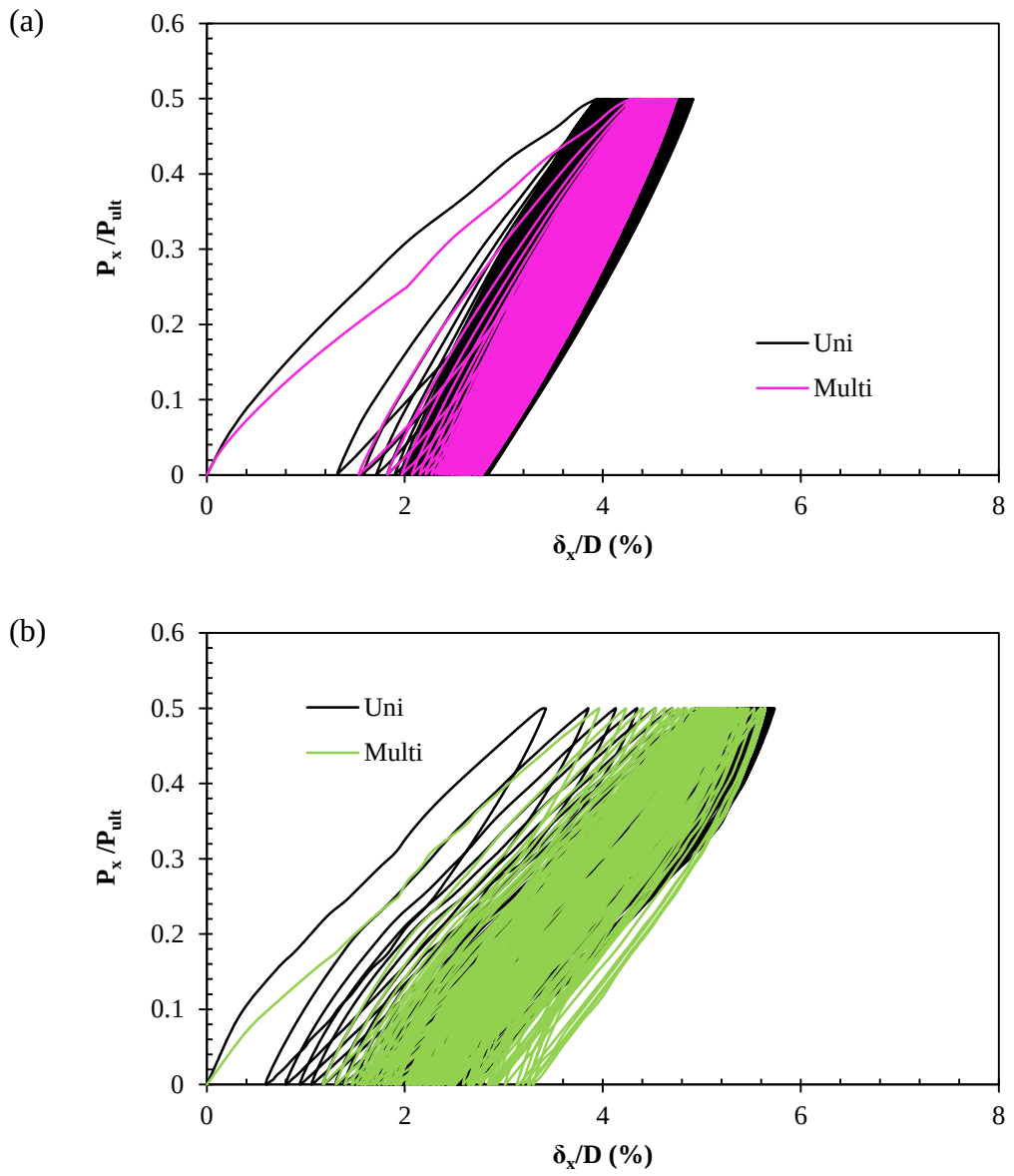

614 **Fig. 12** Comparison of unidirectional and multidirectional P-δ response in the *x*-direction for
615 ζ_c=0 using (a) the HSsmall model and (b) the Hypoplastic model, I_{D0}=0.35

616

617

618

619

620

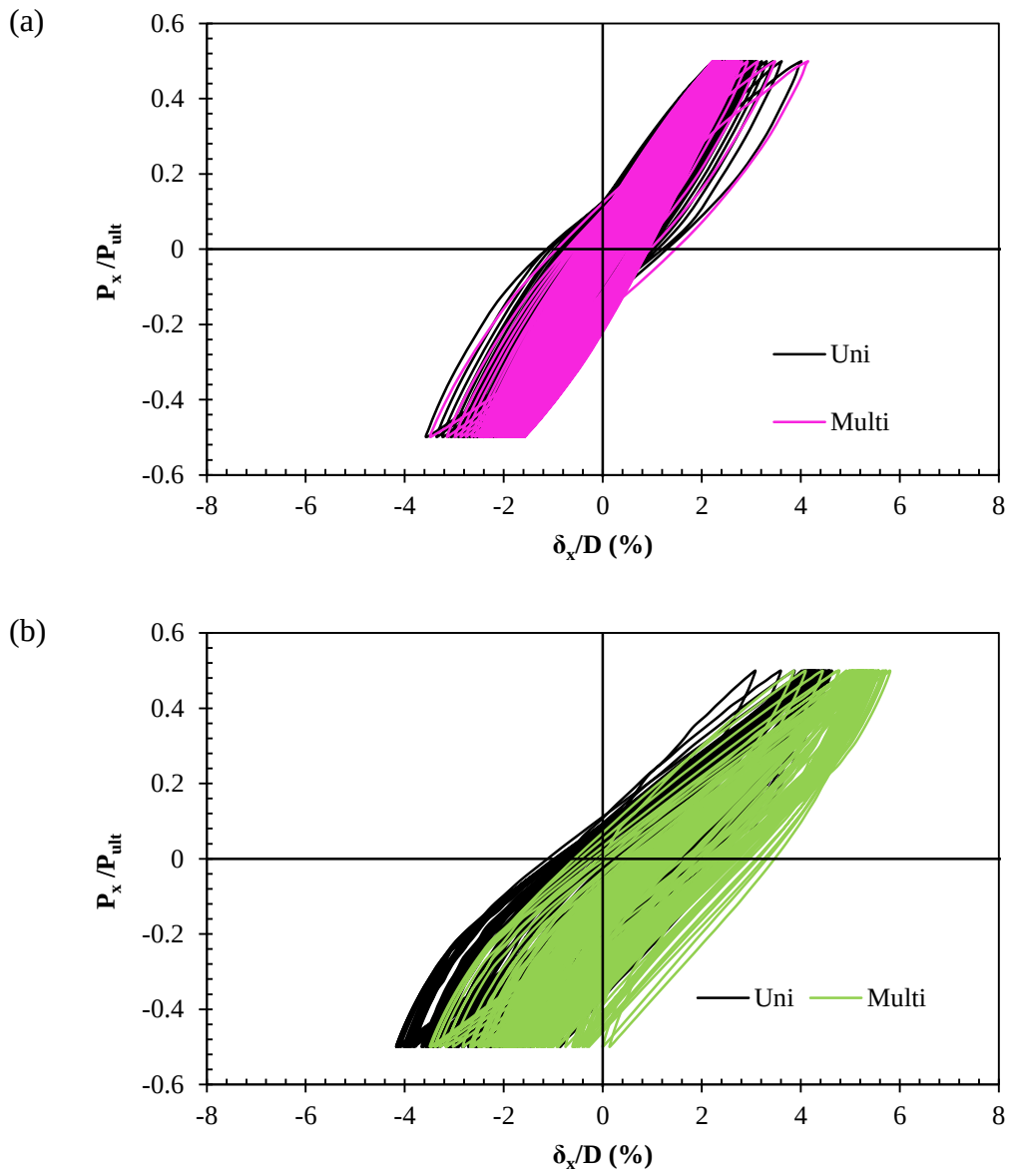

621 **Fig. 13** Comparison of unidirectional and multidirectional P- δ response in the *x*-direction for
622 ζ_c=-1 using (a) the HSsmall model and (b) the Hypoplastic model, I_{D0}=0.35

623

624

625

626

627

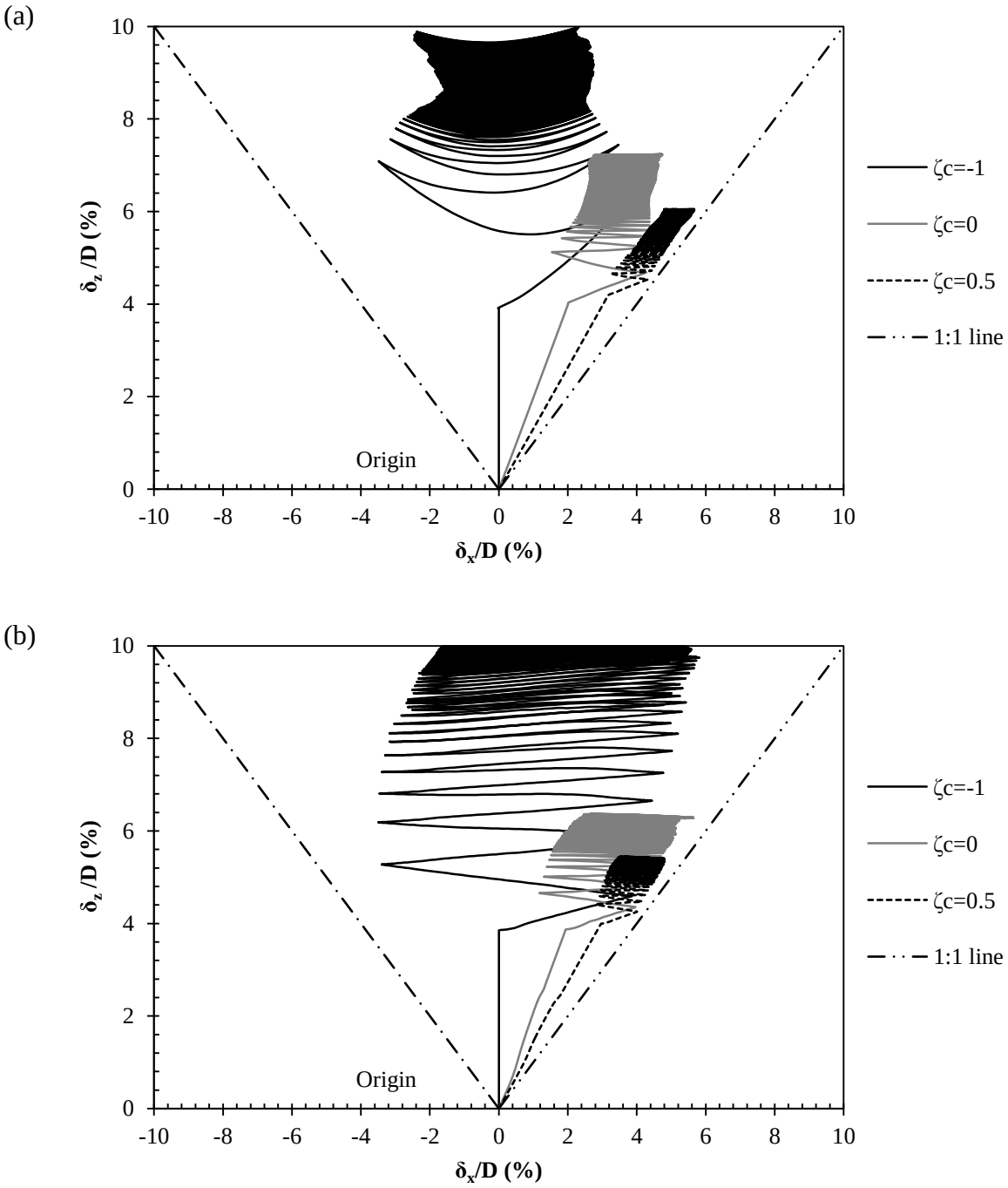

628 **Fig. 14** Multidirectional pile head trajectories using (a) HSsmall and (b) Hypoplastic soil
629 models, I_{D0}=0.35

630

631

632

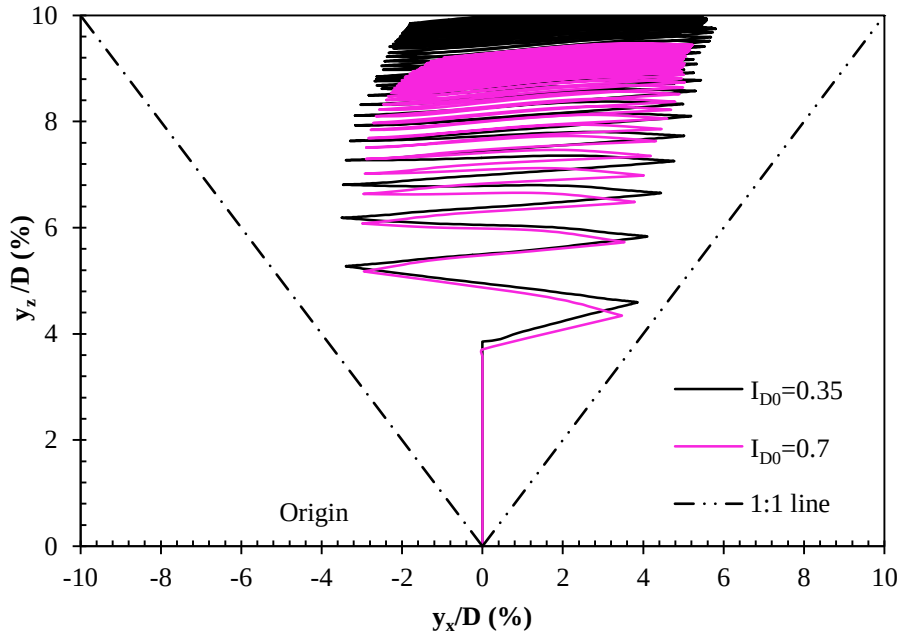

633

634 **Fig. 15** Influence of I_{D0} on multidirectional pile head trajectories using the Hypoplastic soil
635 model
636

637

638

639

640

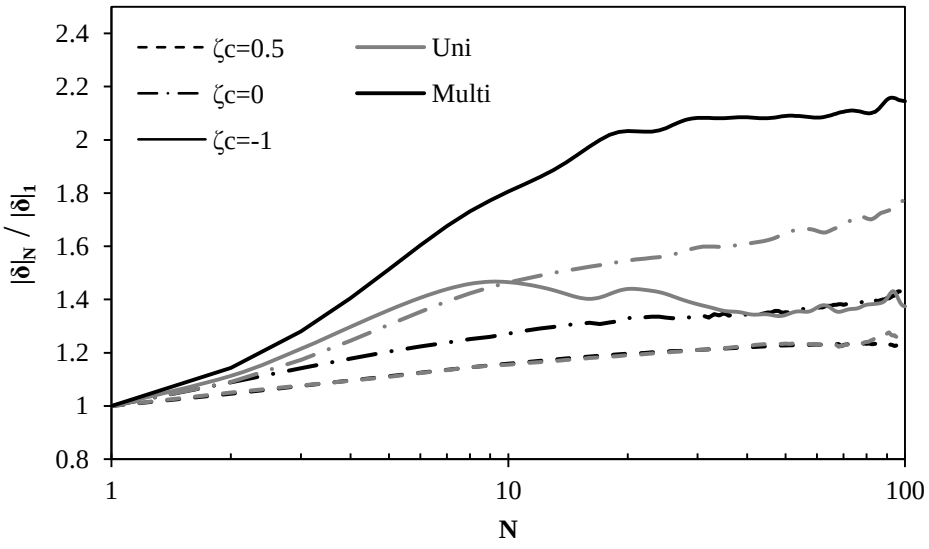

641

642 **Fig. 16** Influence of ζ_c on the variation in accumulated total displacements using the
643 Hypoplastic soil model; I_{D0}=0.35

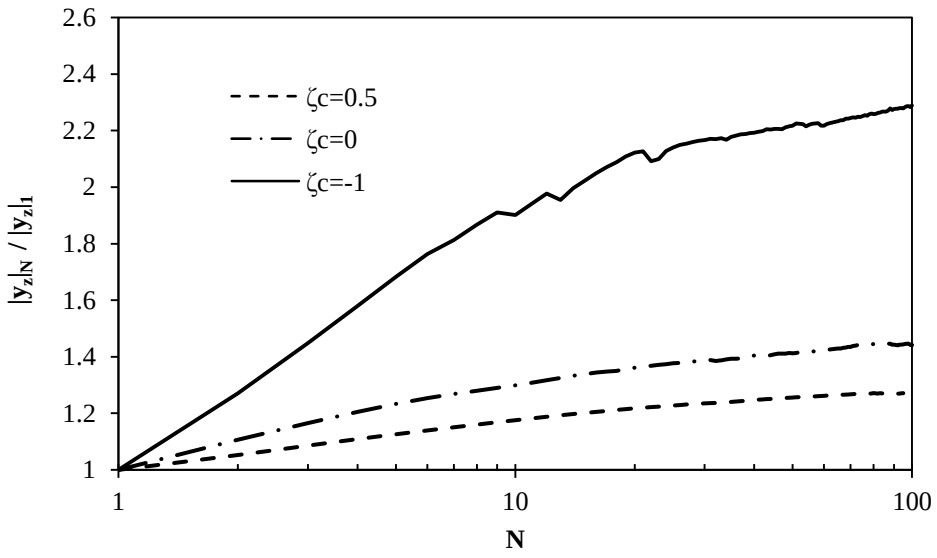

Fig. 17 Influence of ζ_c on the accumulated 'out-of-plane' displacements using the Hypoplastic soil model; I_{D0}=0.35

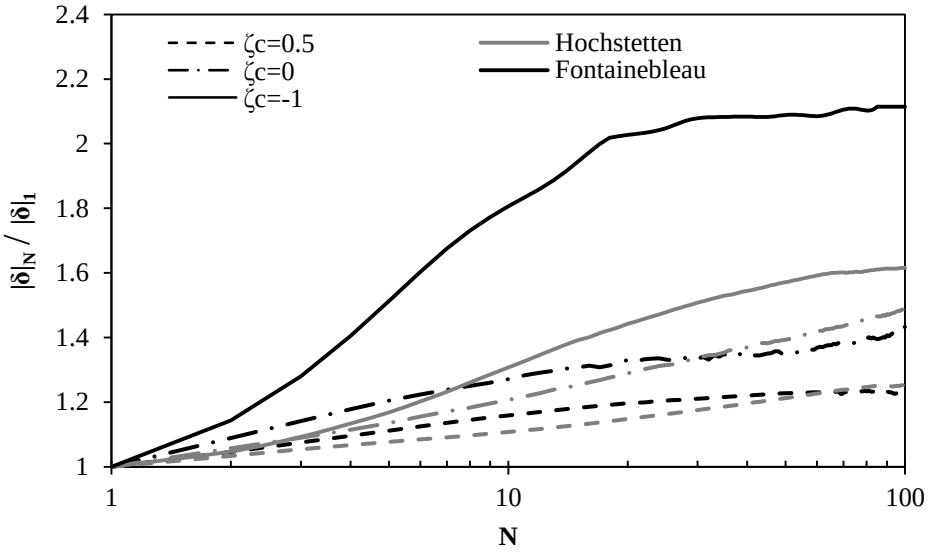

Fig. 18 Influence of sand type on predictions of accumulated total displacements for a variation in ζ_c; multidirectional loading

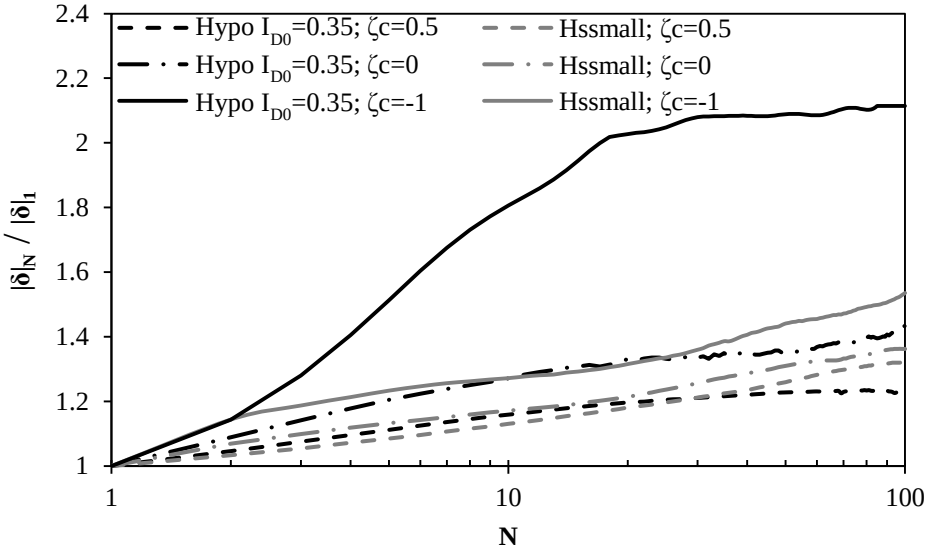

Fig. 19 Influence of constitutive model on predictions of accumulated total displacements for a variation in ζ_c (multidirectional loading)

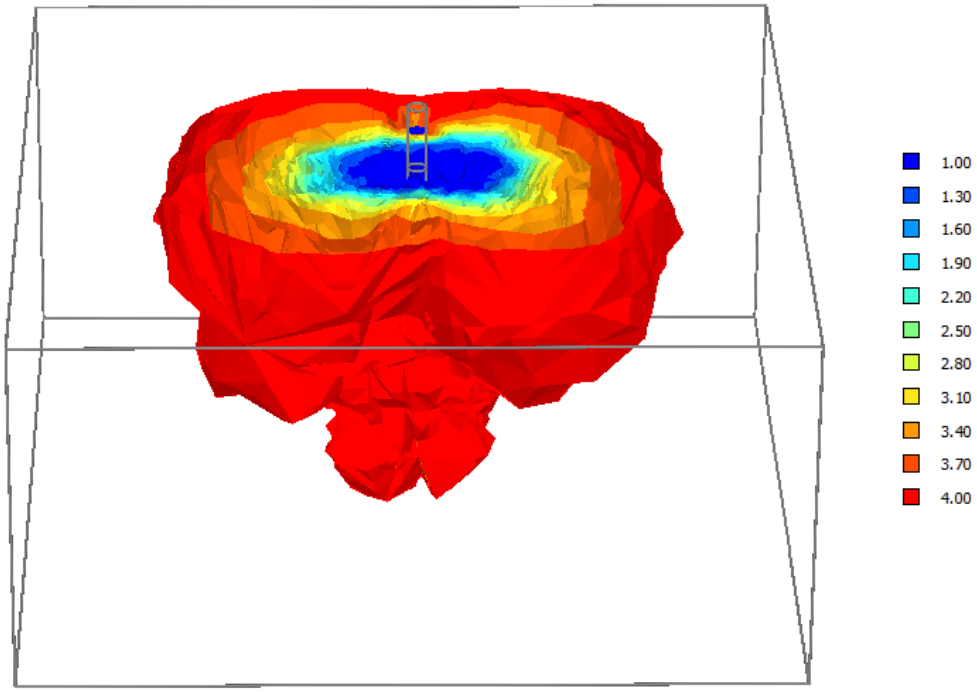

Fig. 20 Three-dimensional contours of *G/Gur* predicted by the HSsmall model; ζ_c=-1, *N*=10

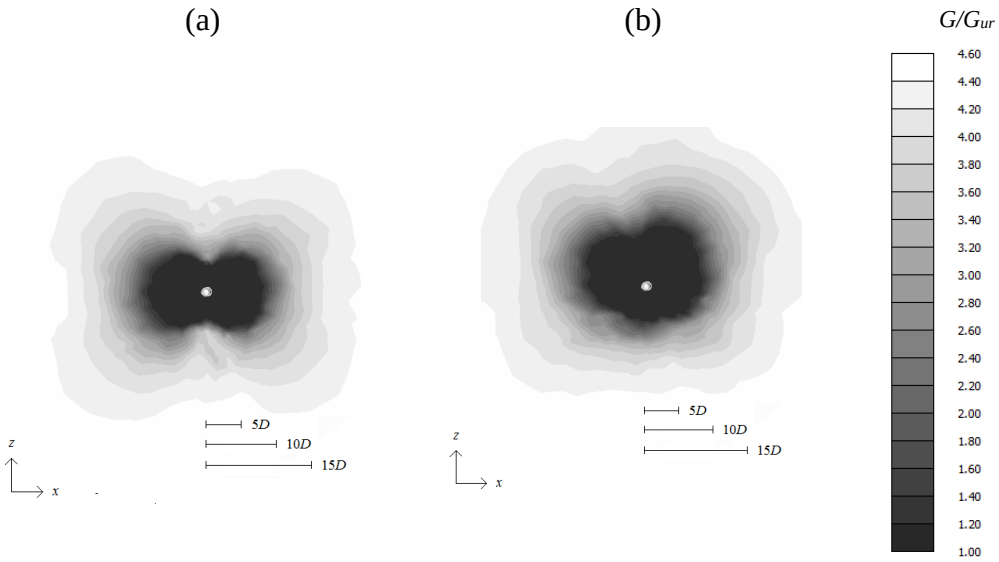

Fig. 21 Contours of G/G_{ur} at ground level for (a) unidirectional *N*=100 and (b) multidirectional *N*=100; ζ_c=-1, HSsmall

(a)

(b)

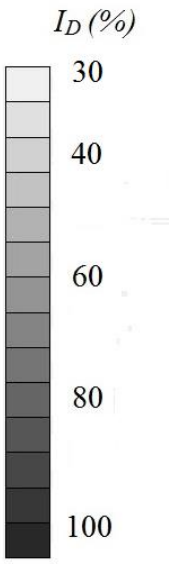

(c)

Fig. 22 Contours of I_D at ground level for (a) multidirectional N=10, (b) multidirectional N=100 and (c) unidirectional N=100; ζ_c=-1, I_{D0}=0.35